Nano-crystal growth in cordierite glass ceramics studied with X-ray scattering

Wim. Bras[1], Simon M. Clark[2], G.Neville. Greaves[3], Martin Kunz[2], Wouter van Beek[4], Velimir Radmilovic[5]

AUTHOR ADDRESS

[1] Netherlands Organization for Scientific Research (NWO)

DUBBLE@ESRF, BP220, F38043, Grenoble Cedex, France

[2] Lawrence Berkeley National Laboratory

1 Cyclotron Road

Berkeley CA 94720-8226, USA.

[3] Department of Physics

University of Wales

Aberystwyth SY23 3 BZ United Kingdom

[4] Swiss-Norwegian Beamlines at ESRF

BP 220 F-38043 Grenoble France

[5]National Center for Electron Microscopy, Lawrence Berkeley National Laboratory, University of California, Berkeley, USA

AUTHOR EMAIL ADDRESS Wim.Bras@esrf.fr

RECEIVED DATE (to be automatically inserted after your manuscript is accepted if required according to the journal that you are submitting your paper to)

CORRESPONDING AUTHOR FOOTNOTE

W. Bras

Wim.Bras@esrf.fr

Tel ++33-476882351

Fax ++ 33-476882412

Wouter van Beek

Dipartimento di Scienze e Tecnologie Avanzate

Università del Piemonte Orientale

A. Avogadro, Via V. Bellini 25/G, 15100 Alessandria, Italy

ABSTRACT

The development of mono-disperse crystalline particles in cordierite glass doped with Cr^{3+} after a two step heat treatment is elucidated by a combination of time-resolved SAXS/WAXS experiments andwith electron microscopy. The effects of bulk and surface crystallization can clearly be distinguished and the crystallization kinetics of the bulk phase is characterized. The internal pressure due to structural differences between the crystalline and amorphous phase is measured but the physical cause of this

pressure can not unambiguously be attributed. The combined measurements comprise a nearly full characterization of the crystallization processes and the resulting sample morphology.

KEYWORDS Cordierite glass, X-ray scattering, Electron Microscopy, Crystallization kinetics.

BRIEFS (WORD Style “BH_Briefs”). If you are submitting your paper to a journal that requires a brief, provide a one-sentence synopsis for inclusion in the Table of Contents.

MANUSCRIPT TEXT (Word Style “TA_Main_Text”).

Introduction

Glass ceramics consist of a glassy matrix in which crystalline nano-crystals are embedded. By tailoring the crystalline compound, both in composition as well as in shape and size, mechanical and optical properties can be influenced. Glass ceramics can be created by a variety of techniques, for example: sol-gel methods, sintering or simple heat treatments[1]. In most glassy materials surface nucleation and crystallization is the dominant process. In order to create a material in which bulk crystallization becomes a factor which influences the final material properties one can use the conventional manufacturing method in which the native glass is doped with a crystallization enhancer and then subject the samples to a two step heat treatment[2, 3]. This method has empirically been developed by manufacturers but the exact mechanism of the crystallization kinetics is still not completely understood[1, 2]. It is well established that this is a method by which relatively monodisperse crystalline particles in an amorphous matrix can be manufactured[4-6]. The amount of dopant will influence the final crystallinity degree. Depending on the type of glass many applications for this kind of composite material can be found in not only the optics industry but also in ceramic heaters, semi-conductor packaging material, catalyst carriers etc. Bulk crystallization can also be induced by bulk inhomogeneities like inclusions, sintering zones or mechanical stress.

Although glass ceramic formation upon heat treatment described in this experiment is widely used in the ceramics industry the basic crystallization processes are still poorly understood[1]. This should hardly be surprising in view of the complicated ternary phase diagram that has been determined for a limited number of isothermal crystallization temperatures [7]. This is not only the case for cordierite but for many other ceramic forming glasses as well.

Glass ceramic based upon a glass with the cordierite composition, $Mg_2Al_4Si_5O_{18}$, is interesting from an engineering point of view since this materials tends to have a low thermal expansion coefficient and excellent mechanical properties, like shock resistance, even at elevated temperatures. This makes it suitable for a variety of applications.

In previous work[4] we have described the crystallization process of a glass with the cordierite composition that was doped with 0.34 mol% Cr_2O_3. Chromium is a well known crystallization enhancer. The glass was subjected to a two step heat treatment in which the samples were first kept at a lower nucleation (or soak) temperature at which Cr is mobile in the glass but the main glass forming network is below the glass transition temperature. With Extended X-Ray Absorption Spectroscopy (EXAFS) it was established that the clustering of the Cr particles creates crystallization nucleation sites which are not able to develop yet into crystallites. By subsequently raising the temperature to a higher level the crystallization can commence. In this way heterogeneous nucleation was induced and the crystallites that form in the glassy matrix are rather monodisperse with a maximum radius of approximately 200 Å which is probably in general dependent on the amount of Cr in the material although this has, so far, not been fully investigated.

In the final material the amorphous glassy phase was still predominant and only around 4% of the material had crystallised in two distinct phases, namely stuffed quartz (μ-cordierite) and spinel. There were clear indications that the spinel phase occurred before the stuffed quartz phase. Therefore these spinel crystallites could act as bulk inhomogenieties which could be the nucleus for the crystallisation of

the stuffed quartz. An alternative mechanism is imaginable in which the two processes are independent and one is bulk nucleation whilst the other starts with surface nucleation.

It is known that undoped cordierite glass hardly has any tendency to form bulk nucleated crystals after heat treatment[8] but that surface nucleation and crystallization are the predominant effects. In this case, up to around 1300ºC, the phase that is formed is the stuffed quartz, or alternatively named 'high quartz or μ-cordierite[9, 10].

In the case that the sample is doped with a crystallisation enhancer, for example: Ti, Fe or Cr, a different situation occurs. In this case bulk crystallisation becomes possible. The phase diagram of glass with the cordierite composition is rather complex and therefore we can not exclude the possibility that a local change in the composition, due to a crystallization event, allows a second phase to be templated upon the original particle. Investigations into the crystallisation velocities of μ-cordierite on impurities in the bulk of the glass compared with surface crystallisation suggest this to be feasible[11]. This could result in composite crystalline particles embedded in a glassy matrix.

In this work we try to shed light on the processes that occur during the crystallization of this particular glass ceramic and on the crystallization kinetics. In particular we have focused on the question if the occurrence of the two crystalline phases is correlated and on the morphology of the material.

Materials and Methods

Time-resolved simultaneous Small and Wide Angle X-ray Scattering (SAXS/WAXS) experiments were carried out on the DUBBLE CRG beam line BM26B at the European Synchrotron Radiation Source in Grenoble[12]. The scattering vector, $q = \frac{4\pi}{\lambda}\sin(\theta/2)$, with λ the X-ray wavelength used and θ

the scattering angle, of the SAXS data was calibrated using a dry rat tail tendon scattering pattern. The WAXS data was calibrated using a Si powder standard. The time framing of the data acquisition system was set to 30 seconds/frame. SAXS data were collected with a multiwire Gabriel type gas detector[13] and WAXS data were collected with a microstrip gas detector[14].

High resolution powder diffraction (HRPD) data were collected, using the powder diffractometer of the Swiss-Norwegian CRG beam line BM01 at the ESRF, in order to accurately characterize the different crystalline phases.. Small angle neutron scattering (SANS) experiments were performed on beam line D22 of the Institute Laue-Langevin in Grenoble. For both these experiments it should be noted that the samples were at room temperature and thus that the unit cell parameters from the distinguishable crystalline phases most likely are somewhat smaller than those determined in the experiments at high temperature due to thermally expansion.

For the time-resolved SAXS/WAXS experiments the sample was placed in a furnace of which the temperature can be controlled with an accuracy of ±2 °C with a maximum estimated temperature gradient over the sample of the same magnitude[15].

The sample preparation method is extensively described in earlier work[4]. After the material was molten and homogenized it was rapidly quenched to room temperature in order to avoid crystallization. The cooled boules were cut into 75 μm thick platelets and slightly polished in order to erase any traces of the sawing process which could artificially increase surface crystallization nucleation.

The samples were subjected to a two step heat treatment. The first stage, at 850º C, was a prolonged heat treatment at a temperature were a maximum number of crystallization nucleation sites were formed[2]. X-ray scattering show that no crystallization or other large scale structures are being formed during this stage. After this initial heat treatment the temperature was raised to 925º C or higher so that

the crystallization nuclei could start to grow. This procedure ensures that we have a well defined initial state which is heterogeneously pre-nucleated regarding crystallization.

Cross-sectional TEM samples were prepared by tripod polishing followed by LN2 cooled low angle ion milling. Bright and dark field images and SAD (selected area diffraction) patterns were taken at 200kV in JEOL 200CX. Energy filtered TEM (FETEM) imaging was performed at 200kV in Philips CM200-FEG TEM equipped with a Gatan Imaging Filter system.

Results

Characterization of the heat treated samples

Although the main aim of our work was to study the time-resolved crystallization process by means of X-ray scattering we have also performed electron microscopy, powder diffraction and Small Angle Neutron Scattering (SANS) on some of the samples that we have used for the X-ray scattering experiments. These results will be discussed here first since it simplifies the subsequent interpretation of the X-ray scattering results.

The reference material that had not been heat treated, or only subjected to the first heat treatment at 850° C, was found to be a homogeneous glass, without any trace of crystallinity, both by powder diffraction as well as by TEM.

For SEM experiments the surface of a freshly broken platelet, without any further sample preparation, was studied. See figure 1.

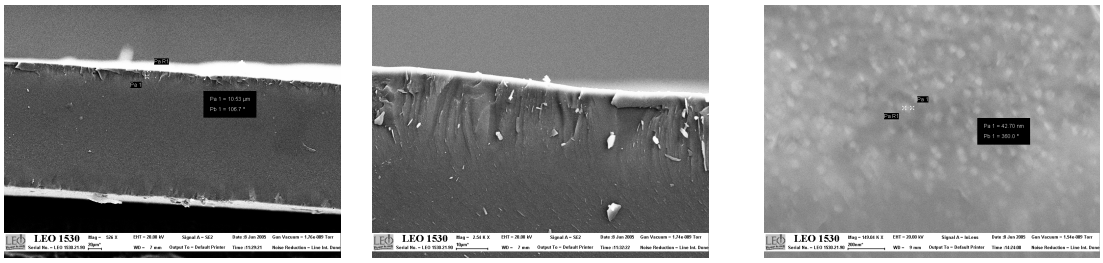

Figure 1 SEM micrographs of a cross section of the sample platelets at different magnifications (respectively from left to right 526, 2540, 149000 times). At the lowest and intermediate magnification of the whole sample and the side it is clear that the structure at the edge of the sample differs from that of the bulk. At the highest magnification we can distinguish in the bulk of the sample the Cr containing spinel nano crystals.

In these SEM micrographs we see that there is a surface layer characterised by conchoidal fractures which is clearly a different structure compared to the bulk. Upon further magnification white dots in the bulk become visible. However, in this case further magnifications proved impossible and the positive identification of the Cr-spinel particles could not be confirmed due to the technical limitations of the technique.

A further investigation on the morphology of the samples was performed with TEM at higher magnifications achievable compared to the SEM. See figure 2.

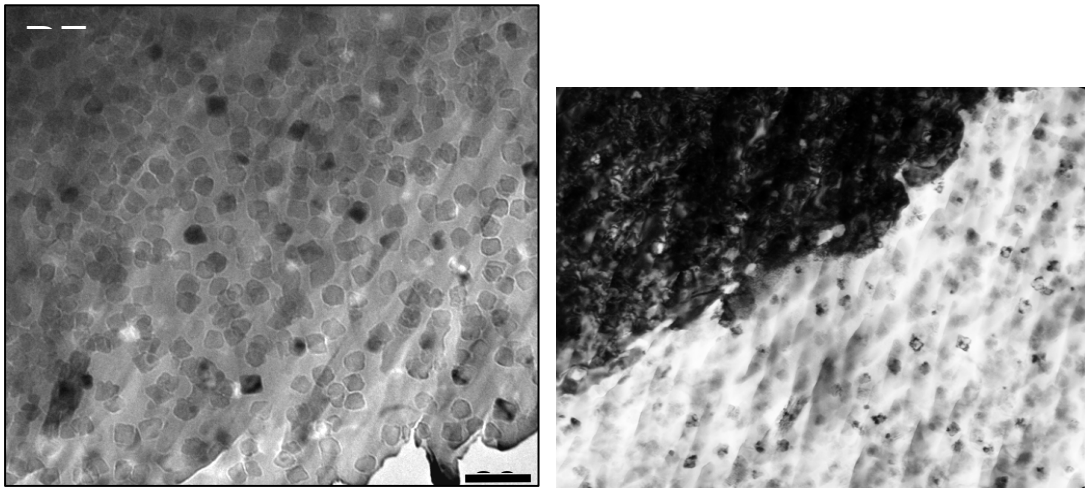

Figure 2

Panel A shows the TEM micrographs of a piece of the bulk of the sample. The black size bar in the right hand corner is 2000 Å long. In these the spinel crystallites are recognizable. In panel B the interface between the surface layer and the bulk of the material is shown at a lower magnification. The striations are due to the sample preparation technique. There is a clear distinction in morphology between the crystalline surface layer and the amorphous matrix.

The TEM graphs show that the bulk of the material is made up of relatively mono-disperse crystallites embedded in a glassy matrix. Some of the crystallites appear to be cubical but more irregular shapes also can be distinguished. Attempts to perform electron diffraction on the small spinel crystallites were not obtained from single particles due to their pronounced rotation in the electron beam. Diffraction data was obtained for some anomalous large spinel crystals in regions where the sample deviated from the normal composition. See figure 3. Energy filter imaging and nanoprobe EDS elemental analysis indeed confirmed the presence of Cr in the spinel crystallites and an absence of Cr in the glassy bulk and the surface layer. It was not possible to obtain electron diffraction from the surface layer.

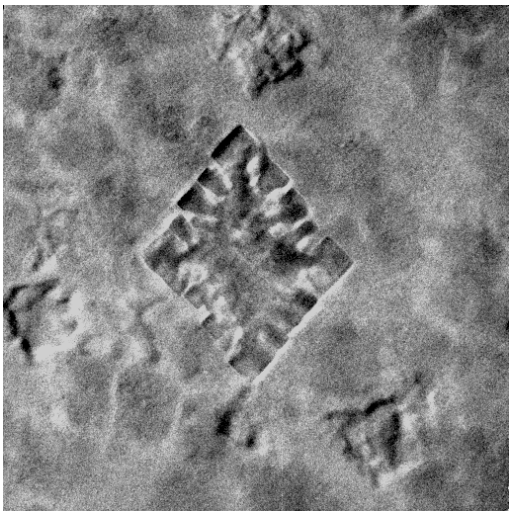

Figure 3

Anomalous large spinel crystal. The particle diagonal is about 1500 Å. Diffraction on all parts of crystallite give the same orientation and confirm a near spinel structure with a unit cell of about 8 A. The lighter parts are amorphous which gives the impression that it is a kind of dendritic growth.

For a more accurate determination of the crystalline components we have performed High Resolution Powder Diffraction (HRPD) on the cooled glass platelets. These experiments confirmed that still a large amount of material consisted of glass. Besides this glass we have been able to determine that there were two crystalline phases present. In the first place a cubic $MgOAl_2O_3$ Cr-spinel with a lattice constant of *8.06 Å* at ambient temperature. This is somewhat smaller then expected for bulk materials but for small crystallites it is known that the lattice constants can deviate from those found in bulk specimens[16-18]. A second phase that was found is a hexagonal stuffed quartz with lattice constants of $a = b = 5.13$ *Å and* $c = 5.37$ *Å* (β-quartz structure with space group P6222) in which, in this case, small amounts of Mg^{2+} are stuffed into the structural channels between the tetrahedral helices. The latter is also known under the name of μ-cordierite[9, 10].

X-ray scattering experiments

In figure 1 we show the time development of the SAXS intensity as function of time obtained during the second step isothermal heat treatment at 925ºC.

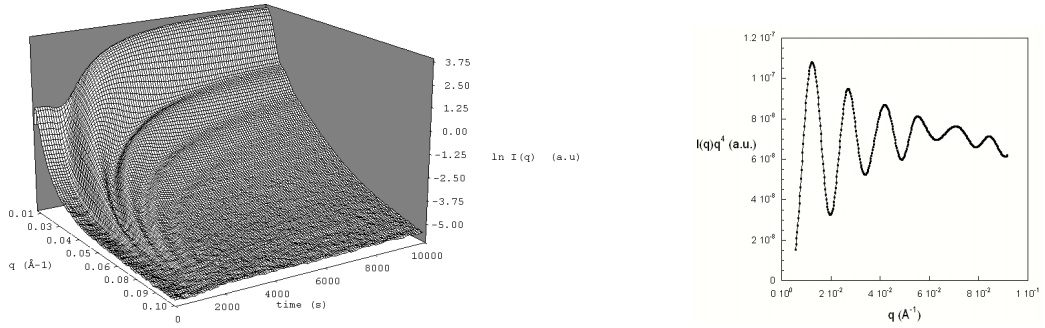

Figure 4

Left panel

Time-resolved SAXS data obtained during the isothermal crystallisation of glass, at 925º C, with the cordierite composition. Time resolution was set to 30 sec/frame. The data are plotted as I(q,t) vs. q and t. The initial intensity is attributed to structure factor scattering[19].

Right panel

Averaged data from 10 frames obtained during the final stages of crystallisation. The data is plotted as $I(q)q^4$vs q. The peak around q = 0.01 $Å^{-1}$ can be attributed to be structure factor scattering. The other maxima fall within the error margin on a curve that represents the form factor scatter[19] from a uniform spherical scatterer.

At the initial stage during the pre-heating or soak stage, no structure can be observed. However, several minutes after the sample has reached the higher equilibrium temperature the SAXS intensity starts to increase profoundly. A shallow peak appears at low *q*. In time this moves only slightly to lower *q* values. However, several other peaks can be distinguished which all move in time towards lower *q*. At

later stages we can actually distinguish five discrete scattering maxima which is only limited by the finite size of the detector[13].

The intensity in the SAXS regime is given by[20]:

$$I(q) = S(q)\left|F(q)\right|^2 \qquad [1]$$

In which *S(q)* is the structure factor scatter due to the existence of spatial correlations among the scattering entities in the amorphous matrix. *F(q)* is the form factor which depends on the shape and size of the scattering entities[19]. The striking observation here is that there are many form factor scattering fringes visible even though the TEM micrographs indicated that there was no complete shape homogeneity. This indicates that the scattering entities are rather monodisperse in size.

The first peak in the scattering pattern emerges before the other peaks and, in contrast to the later occurring intensity maxima, remains approximately in the same position. The fact that this only moves slightly towards lower *q* in time combined with the knowledge that the particles are rather monodisperse in size indicates that we are dealing with a system in which the increase in size of the particles is due to a growth process and not to an agglomeration of individual particles. This is in agreement with the assumption that only during the pre-heat treatment crystallisation nucleation sites have been created.

The structure factor peak maximum is at later stages dominated by the intensity due to the form factor but estimated to stabilize at a scattering vector value of $(4 \pm 1) \times 10^{-3}$ Å^{-1}. This value agrees reasonably well with the average distance between scattering particles which can be assessed from the TEM data. See figure 1a. This with the understanding that there is only a limited accuracy in the TEM data in this respect since we see a three dimensional structure projected upon a plane. When we combine the thus derived particle interdistance with the information on the final radius of the particle we can asses that the final volume fraction of particles giving rise to form factor scattering is approximately 1 %. Given

the indirectness of this method it is in reasonable agreement with earlier experiments and simulations[21, 22]. After cooling down SANS measurements only showed the structure factor peak and no form factor fringes. This is in agreement with earlier SANS experiments[22].

Our data fits, within the error margins, the form factor scatter of spherical scatterers with a smooth and sharp surface[20]:

$$F(q) = \frac{3\left(\sin qR - qR\cos qR\right)}{\left(qR\right)^3} \qquad [2]$$

Using this expression we can approximate the particle size evolution in time. We remark here that for this procedure the limited active length of the detector prevents more than one fringe to be observable for the smaller particles, and that for larger particles, where the minima in the curves are much closer, the limited spatial resolution of the detector limits the accuracy. Also we have shown in earlier work that the interface between the scattering entities and the matrix is not completely sharp but that there is a small diffusion zone around the particles which is depleted from Cr. These facts, in combination with the limited counting statistics intrinsic to this type of time-resolved data, also allow us to match the time-resolved data to cuboidal form factors.

Numerical simulations show that scattering curves from an assembly of slightly polydisperse spheres are nearly indistinguishable from those of more monodisperse cuboids. For the time-resolved data we found that it was not possible to find a satisfying method to study the polydispersity. In order to still obtain an estimate of the total polydispersity, for as far as this is possible for scattering entities without complete shape homogeneity, we averaged 10 data frames obtained when the particle size had stopped increasing and performed an analysis using conventional methods[23]. Unfortunately this rendered results in which the error margin was larger than the measured parameter. Therefore we have resorted to a method that can be used for rather monodisperse spherical particles. Here the scattering fringes are still discernible but decay at a rate faster than for a completely monodisperse system[24]. We find that the

polydispersity is around $\Delta R / R = 0.03 \pm 0.01$ if we assume that the particles are spherical and have sharp interfaces with respect to the surrounding matrix. For any other morphology, where the scattering fringe decay is more rapid than for spherical particles, this indicates that the size distribution range will be even narrower.

In the simultaneously performed WAXS experiments we can observe the growth of the two crystalline phases. See figure 5. The resolution of the position sensitive detector used in these time-resolved experiments is not high enough to be able to determine the phases, unit cell parameters or the exact composition accurately. For this we rely on the HRPD experiments discussed above. However, the changes in lattice spacing and diffraction intensities during the growth process can be followed on a time scale that is not possible with a conventional diffractometer set-up.

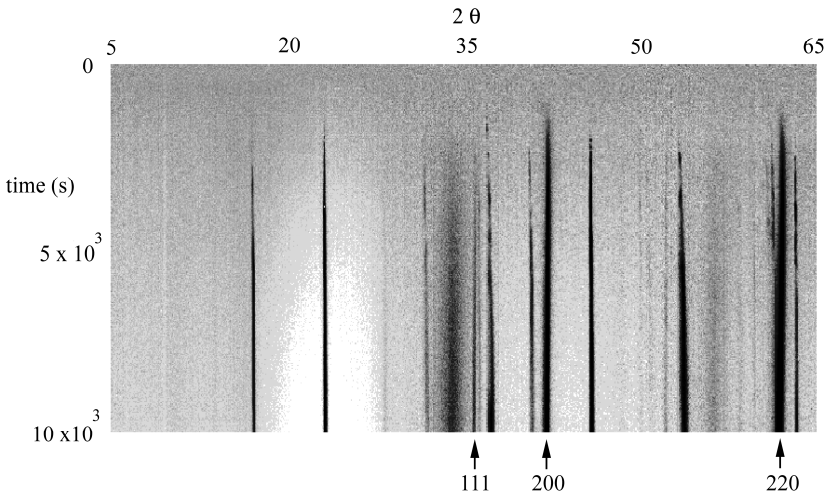

Figure 5.

Diffraction pattern development during the isothermal treatment at 925º C. Two different crystalline phases develop. The peaks that can be attributed to the spinel phase are indicated by arrows. The remaining peaks are all due to the stuffed quartz phase. Diffraction peaks that can be indexed to the

spinel phase all increase monotonically in time and show a shift to lower angle, indicating an increase in the unit cell size. The development of the stuffed quartz peaks is more complex.

The time-resolved experiments do reveal that the lattice constants for both crystalline phases are not fixed during the experiment but do change considerably during the isothermal heat treatment and particle growth regime.

The most sensitive parameter to determine if any structural changes are occurring in a sample is in general the total scattering intensity or invariant which for a multiphase isotropically scattering system can be written[25]:

$$Q = C_1 \int_0^{\infty} q^2 I(q) dq = C_2 \sum_{i \neq j} \phi_i \phi_j \left[\rho_{ei} - \rho_{ej} \right]^2 \qquad [3]$$

In this $C_{1,2}$ are constants, ϕ_i is the volume fraction of component i and ρ_{ei} is the electron density of the phases. In figure 6 we plot the development of the invariant and the integrated peak intensity for representative WAXS peaks for the two different phases.

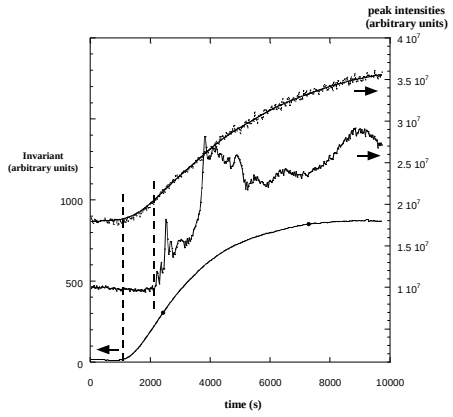

Figure 6

Time-development of SAXS intensity (bottom curve) co-plotted with the integrated intensity of a representative diffraction peak of the spinel phase (top curve) and the integrated intensity of the first quartz peak that appeared (middle curve). The arrows indicate the intensity scales. The error bar for the integrated intensity is smaller than the symbol size. For the crystalline peaks all data points have been

plotted which gives an indication of the error margin. The sample was pre treated at a T=850º C and then crystallized at T=1025º C. The irregularity in increase is observed for all stuffed quartz peaks.

It is clear that the increase in the invariant and the spinel starts at the same time and that the stuffed quartz begins to form at a later time. The irregular increase in the intensity of the stuffed quartz confirms that this is the crystalline phase that develops on the surface. The irregularity is due to the development of a surface texture which is continuously being modified as growing crystallites with slightly different orientations impinge upon each other. Depending on the small changes induced in the orientation of the individual crystallites by this impingement different peaks can in- or decrease in intensity.

The fact that we observe several interference fringes in the SAXS pattern allows us to calculate the size of the particles with a higher degree of accuracy then when having to revert to the determination of the radius of gyration. This with the caveat that the scattering entities are not completely homogeneous in shape and that therefore the average dimension will be in between those calculated assuming a spherical form factor and a cuboidal form factor. In figure 7 the development of the particle size is co-plotted with the spinel axis size. At the initial stages the error margin in the size determination is less than 2%. This increases to about 5% when the particles increase in size due to the limited spatial resolution of the detector.

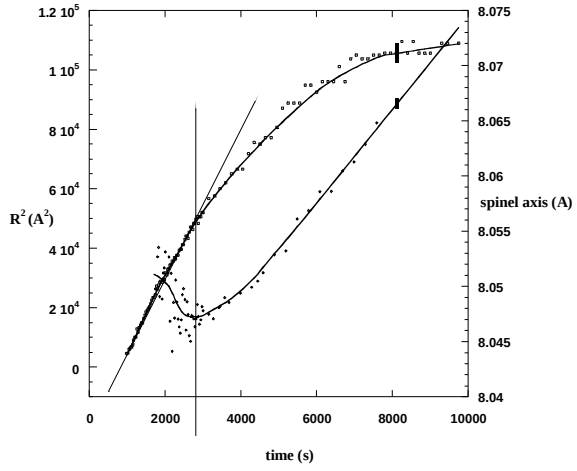

Figure 7

The correlation between the R^2 of the particle versus time (square symbols). The vertical bars at time = 8000 sec indicate the error margins at the later stages of development. At the early stages a linear fit can be made to the R^2 data. This confirms the predictions that we are dealing with a diffusion limited growth process. The development of the spinel unit cell volume as function of time (diamond symbols). The changeover from shrinking to growing coincides with the moment when the particle size leaves the $\sqrt{t}$ growth regime. Also noteworthy is that this is the moment when the noise is much reduced.

We note here that in the early stages the increase in particle size can be described by the relation $R(t) = C\sqrt{t}$. In figure 7 we have also plotted the length of the spinel unit cell axis. At low degrees of crystallinity the exact position of the diffraction peaks, and thus the size of the axis, is more difficult to determine then the total integrated peak intensity which is plotted in figure 6. However, at the very early stages there is a tendency for the axis to shrink. This process is reversed at the moment that the crystal growth starts to slow down. After that we observe a linear increase in unit cell length. Unfortunately, due to the limited time available, the experiments were not continued for long enough to know what the equilibrium size would be.

We have also found that the shape of the unit cell of the stuffed quartz phase changes in time. The development of the axis is plotted in figure 8.

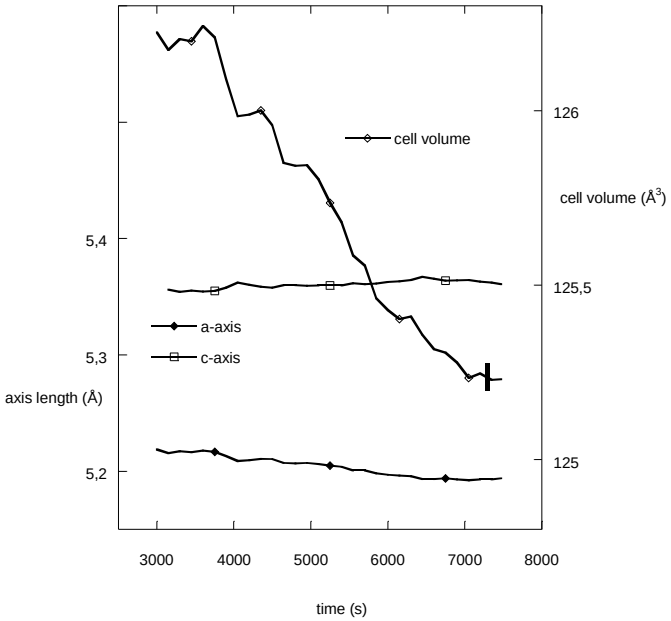

Figure 8

The time development of the unit cell parameters of the stuffed quartz, or μ-cordierite, unit cell during isothermal crystallization. The error bar on the a and c axis at the later stages of development is roughly the size of the symbols. The error bar on the unit cell volume is given by the vertical bar.

It can be seen that in time there is a slow extension of the unit cell with the basal plane shrinking but the long axis extending. The total unit cell volume, however, only varies less than a percent.

A conventional tool for the analysis of crystallization kinetics is the Avrami formalism or one of the related analysis techniques. In this formalism the change in crystalline volume fraction is related to parameters like the dimensionality of the growth and the growth mechanism, i.e. diffusion or reaction limited growth.

$$V_c = 1 - e^{-(kt)^n} \qquad [4]$$

where V_c is the crystalline volume fraction, *k* a constant that depends on nucleation rate and structural relation time and *n* relates to the nature of the growth process[26].

The integrated peak intensity of a diffraction peak has a linear relation with the crystalline volume fraction in a sample: $V_c(t) \approx C\int_{q_1}^{q_2} I(q,t)dq$. Therefore we can fit this intensity to the Avrami equation. The parameter, *n*, relevant for the nature of the growth process, derived from this fit is $n = 1.49 \pm 0.01$. A single determination of parameters like this is prone to systematic errors. However, a cross correlation is possible. We already have established that the spinel particles are monodisperse within a few percent. In earlier work we have shown that the number of particles, *N*, is also fixed. Therefore the number of particles multiplied by the cubed radius of the particle is also a measure of the crystalline volume fraction: $V_c(t) \approx N(R(t))^3$. This data set renders $n = 1.51 \pm 0.05$. Both fits, from simultaneous but independent experiments, give an Avrami exponent that within the error margin is identical. For a pre-nucleated system with three dimensional growth this value of *n* indicates that the particle growth takes place via a diffusion limited growth process[26]. In diffusion limited processes the growth rate of the particles in the early stages should be proportional to the square root of time[22, 27].

As can be seen in figure 7 this behavior is indeed observed. Thus we have three analysis methods from two independent experiments that confirm that the spinel growth is a diffusion limited process.

From the SAXS data we can still derive some further information about the growth process. Keeping in mind that the pre-heat treatment created crystallization nucleation sites that were only growth activated upon raising the temperature and that we have shown that we are dealing with a diffusion limited growth process we can assume that the development of the particle radius will have the following time and temperature dependence:

$$R^2 = \frac{2C_i D(T)t}{\rho} \qquad [5]$$

in which R is the radius of the spherical particle, ρ the density of the particles in 'concentration units', C_i the initial Cr concentration in the starting glass and $D(T)$ the temperature dependent diffusion constant[28, 29].

Using equation 2 we can express $D(T)$ as a function of experimentally determined parameters combined with sample preparation parameters. The diffusivity is temperature dependent according to:

$$D(T) = D_0 e^{-\frac{Q_a}{RT}} \qquad [6]$$

where R is the gas constant and Q_a the activation energy.

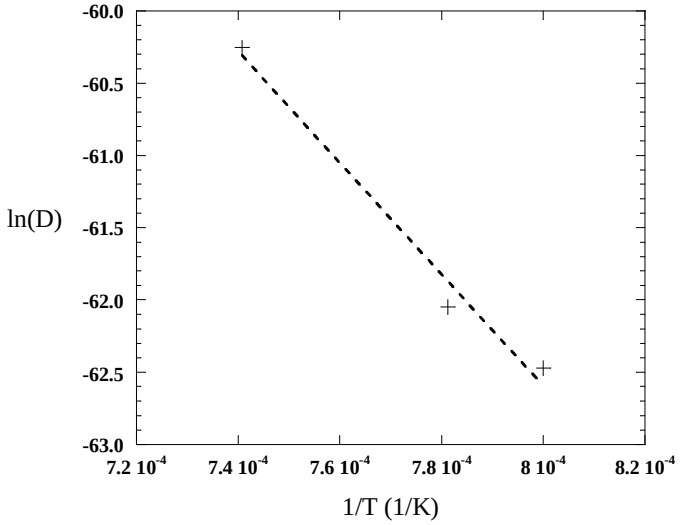

Figure 9

Arrhenius plot of the diffusivity versus inverse temperature. The dashed line is a linear fit to the data. Based upon this data the activation energy can be determined.

The activation energy, Q_a, is determined to be 5.0(3) 10^{-18} JK^{-1} - this is 3.3 eV, which is a factor 2 lower than the value found with Thermal Analysis for a Ti containing cordierite[30] and in good agreement

with similar other systems[6]. We remark here that for the surface crystallization process, which starts later then the bulk spinel formation, an activation energy for powdered samples was found by thermal analysis techniques, that is approximately a factor 10 higher[31]. The actual value depended on the powder particle size range.

In figure 8 we have also plotted the evolution of the spinel unit cell axis as function of time. This has a somewhat puzzling behavior. After an initial decrease in the unit cell size we observe an increase which is linear in time. These slight changes are of second order importance with respect to the actual size of the individual crystallites during the growth process. These show a continuous increase due to the continuation of the crystallization process at the outer surfaces with respect to the glassy matrix.

The relative deformation of the unit cell indicates that either a positive or negative pressure is exerted on the crystallites. The magnitude of this pressure felt by the spinel spheres can be estimated using a 2nd order Birch-Murnaghan equation of state[32]

$$P = 1.5 \cdot K_{0,1050}\left[\left(\frac{V_{0,1050}}{V}\right)^{7/3} - \left(\frac{V_{0,1050}}{V}\right)^{5/3}\right] \qquad [7]$$

with $K_{0,1050}$ representing the isothermal bulk-modulus at 1050º C, $V_{0,1050}$ the zero-pressure volume at 1050ºC. We assumed values for $K_{0,1050}$ and $V_{0,1050}$ of 175 Gpa and 548.689 $Å^3$, respectively[33, 34]. We realize that these values may not represent the proper base values for a nano-crystalline spinel, and the absolute pressure inferred may thus not be accurate. However, since the bulk modulus of the nano-particle is likely not to be greatly different from its bulk equivalent, the obtained changes in pressure reflect a correct ballpark figure. The high-temperature unit cell metric is deduced using an ambient temperature value for a_0 of 8.187 Å and a thermal expansion coefficient $\alpha \approx 9.6\times10^{-6} K^{-1}$ with $a_T = a_0(1+\alpha\Delta T)$ and the assumption that 20% of the Al^{3+} on the octahedral sites will be replaced by

Cr^{3+} with an 0.08 Å larger ionic radius. This leads to an initial pressure around 9.5 GPa, which rises to ~ 10 GPa before monotonically dropping to ~ 8.5 GPa.

Discussion

In earlier experiments[4] we have already established that in Cr doped glass with the cordierite composition, which were subjected to a two step heat treatment, two crystalline phases occurred. Using only X-ray scattering it was not possible to determine if the growth of these phases were correlated or not. By using TEM and SEM we have been able to show the existence of a stuffed quartz surface layer, spinel crystallites in the bulk and a remaining glass matrix which makes up the largest part of the volume. This morphology tells us that the growth of the crystalline phases is uncorrelated. It is plausible that if the samples are kept longer at the elevated temperatures ultimately the whole glass matrix will be converted to stuffed quartz.

Previously we have also found that only during a limited time there were several scattering fringes visible in the SAXS pattern during the isothermal heat treatment[4] whilst in the present work these fringes are visible throughout the experiment. This discrepancy can be explained by the fact that in the most recent results we have utilized a sample furnace which limits the temperature gradient over the sample. For the interpretation of the kinetic results the difference is crucial. Where in earlier instances we were not able to analyze the data with the conventional mathematical tools we have now been able to show that in the case of the spinel growth both the SAXS as well as the WAXS data show that the process is diffusion limited.

The growth of the stuffed quartz phase can not be studied quantitatively in this case due to the changing texture of the surface giving rise to an irregular increase in the diffraction peaks. In principle

one would be able to overcome this problem by using a powdered sample instead of a platelet but it has been shown that the coarseness of the powder influences the crystallization kinetics[31]. However, this is beyond the subject of this study. The fact that this has not been observed in our earlier work can be explained by sample temperature gradients and by the fact that previously the samples had not been polished. The combination of the non-smoothness of the sample surface and the temperature gradient has brought about an apparent orientational randomization of the surface crystallites.

During the growth of the stuffed quartz we observe that the basal plane is shrinking and that the long axis extending. The total cell volume, however, only varies less than a percent. The observation that a textured crystalline surface layer appears has been made previously[11]. These authors found that for μ-cordierite the speed of growth along the *c*-axis is nearly twice as large as in the *a*-axis direction. Moreover it was established that in crystals that are oriented with their *c*-axis parallel to the surface the ratio is even higher. There are multiple nucleation sites on the surface. Once the different crystals impinge upon each other and the surface is completely covered the crystallites with their *c*-axis pointing into the bulk become the fastest growing species. This has also been observed in other low thermal expansion coefficient glass ceramics[35]. It therefore is no surprise that during this growth process, with a changing texture, the intensity of the diffraction peaks can vary quite erratically even though the position of the diffraction peaks show a much smoother variation.

The measured unit cell of the spinel phase is significantly smaller than what would be expected for a bulk spinel crystal of the present composition at ambient conditions. In general the lattice parameters of nano crystals increase as a function of decreasing particle size [36]. However, also some cases are known where the inverse is true [37, 38]. In addition to this off-set of lattice parameters we also observe a continuous change of the unit cell parameters during the crystallisation and growth process of the spinel phase. The initial relative increase in the spinel unit cell size can be explained by the assumption that the density of the crystallizing spinel is higher than the density of the surrounding amorphous matrix. We

assume this based on the change in composition from a chromate-rich nucleating site to the final composition of $(MgCr_2O_4)_{0.18}(MgAl_2O_4)_{0.82}$ on one hand, and to the general observation of a decrease in density upon amorphisation. Therefore there is an incompatibility in the specific volumes occupied by the amorphous matrix and the spinel crystallized out of it[15]. The consequence of this is that a negative, i.e. pulling, force is exerted on the growing crystallites. Interestingly the inflection point of decrease to increase of the unit cell parameter coincides with the moment that the particle growth rate leaves the parabolic regime. In earlier experiments we have noticed that this is the moment as well when the Porod slope increases from a rather low value of around 1.5 to a value of 4. Although there are several morphologies that can generate power law scattering this behavior is generally found at lower scattering angles than discussed here. In the scattering vector regime $q \to \infty$ this intensity is mainly due to particle surface roughness. Here it indicates that the particles become smoother[20]. The most likely explanation is that in the early stages new material is added so rapidly that there is a competition between the process in which the surface of the particle with respect to the surrounding matrix is minimized and the addition of new material. When the matrix becomes depleted the growth rates diminish and the particle becomes smoother.

In earlier experiments we have found that the scattering invariant, *Q*, kept increasing even after the radius of the scattering particles had stopped increasing. For a fixed number of monodisperse particles an increase in the invariant can not be true after the particles have stopped growing. However, if we leave the notion of a two phase system but instead interpret the facts in the light of a three phase system it becomes understandable. Referring to equation 3 we can see that the extra contribution to the invariant, *Q*, is entirely due to the creation and increase in the surface/volume between the amorphous phase and the stuffed quartz whilst the contribution of the spinel/amorphous phase remains constant.

Conclusions

The combination of TEM, SEM and time-resolved combined SAXS/WAXS techniques has allowed us to characterize the temperature induced crystallization of Cr doped cordierite glass. We have shown that the growth of the two crystalline phases is independent of each other and that not one of the phases acts as the template for the other but that we can distinguish between bulk and surface crystallization.

By using the Avrami formalism we have shown that the bulk spinel phase grows by a diffusion limited process. It is surprising to see that even though the crystallites are not completely homogeneous in shape it still was possible to distinguish several SAXS form factor fringes. This has allowed us to obtain an estimate of the particle size polydispersity.

It has become clear that the sample geometry is of importance and that with platelet like samples one can distinguish between the surface and bulk crystallization process. This is something that would not be feasible with powdered samples. However, in the platelet geometry it is not possible to derive quantitative results on the kinetics of the surface crystallization.

Acknowledgements

Alex Korsunsky and Menno Oversluizen are acknowledged for discussions, Ray Jones, Igor Dolbnya, Ruud van Tol and Dirk Detollenaere for technical assistance. Stuart Clarke for obtaining the SANS data, Irina Snigireva for making the SEM pictures of the samples, Claudio Ferrero for calculations and Florian Meneau for assistance in the data reduction. The Netherlands Organization for Scientific Research (NWO) is thanked for making access to BM26B at the ESRF possible. All transmission electron microscopy characterization has been performed at the National Center for Electron Microscopy at Berkeley and was supported by the Director, Office of Science, Office of Basic Energy Sciences, of the US Department of Energy under Contract No. DE-AC02-05CH11231. the referees are thanked for

useful suggestions on the restructuring of the manuscript. Ulrich Dahmen is thanked for fruitful discussions and Howard Padmore for creating the possibility to spend time at the ALS.

References

(1) James, P. F., Glass-Ceramics - New Compositions and Uses. *Journal of Non-Crystalline Solids* **1995,** 181, (1-2), 1-15.

(2) Jong, B. d.; Adams, J.; Aitken, B.; Dickenson, J.; Fine, G., *Ullman's Encyclopedia of Industrial Chemistry 5th ed. Wiley* **1989,** A12, 433.

(3) Karamanov, A.; Cantalini, C.; Pelino, M.; Hreglich, A., Kinetics of phase formation in Jarosite glass ceramics. *Journal of the European Ceramic Society* **1999,** 19, 527-533.

(4) Bras, W.; Greaves, G. N.; Oversluizen, M.; Clark, S. M.; Eeckhaut, G., The development of monodispersed alumino-chromate spinel nanoparticles in doped cordierite glass, studied by in situ X-ray small and wide angle scattering, and chromium X-ray spectroscopy. *Journal of Non-Crystalline Solids* **2005,** 351, (27-29), 2178-2193.

(5) Craievich, A. F.; Kellermann, G.; Barbosa, L. C.; Alves, O. L., Structure characterization and mechanism of growth of PbTe nanocrystals embedded in a silicate glass. *Physical Review Letters* **2002,** 89, (23).

(6) Kellermann, G.; Craievich, A. F., Isothermal aggregation of Ag atoms in sodium borate glass. *Physical Review B* **2004,** 70, (5).

(7) Schreyer, W.; Schairer, J. F., Compositions and Structural States of Anhydrous Mg-Cordierites - a Re-Investigation of the Central Part of the System Mgo-Al2o3-Sio2. *Journal of Petrology* **1961,** 2, (3), 324-406.

(8) Muller, R., Surface nucleation in cordierite glass. *Journal of Non-Crystalline Solids* **1997,** 219, 110-118.

(9) Schreyer, W.; Schairer, J., Metastable solid solutions with qurtz-type structures on the join SiO2-MgAl2O4. *Zeitschrift fur Kristallographie* **1961,** 116, 60-82.

(10) Muller, R.; Naumann, R.; Reinsch, S., Surface nucleation of mu-cordierite in cordierite glass: Thermodynamic aspects. *Thermochimica Acta* **1996,** 280, 191-204.

(11) Diaz-Mora, N.; Zanotto, E. D.; Hergt, R.; Muller, R., Surface crystallization and texture in cordierite glasses. *Journal of Non-Crystalline Solids* **2000,** 273, (1-3), 81-93.

(12) Bras, W.; Dolbnya, I. P.; Detollenaere, D.; van Tol, R.; Malfois, M.; Greaves, G. N.; Ryan, A. J.; Heeley, E., Recent experiments on a combined small-angle/wide-angle X-ray scattering beam line at the ESRF. *Journal of Applied Crystallography* **2003,** 36, 791-794.

(13) Gabriel, A.; Dauvergne, F., *Nuclear Instruments and Methods* **1982,** 201, 223.

(14) Dolbnya, I. P.; Alberda, H.; Hartjes, F. G.; Udo, F.; Bakker, R. E.; Konijnenburg, M.; Homan, E.; Cerjak, I.; Goedtkindt, P.; Bras, W., A fast position sensitive microstrip-gas-chamber detector at high count rate operation. *Review of Scientific Instruments* **2002,** 73, (11), 3754-3758.

(15) Sankar, G.; Wright, P. A.; Natarajan, S.; Thomas, J. M.; Greaves, G. N.; Dent, A. J.; Dobson, B. R.; Ramsdale, C. A.; Jones, R. H., Combined Quexafs-Xrd - a New Technique in High-Temperature Materials Chemistry - an Illustrative in-Situ Study of the Zinc Oxide-Enhanced Solid-State Production of Cordierite from a Precursor Zeolite. *Journal of Physical Chemistry* **1993,** 97, (38), 9550-9554.

(16) Gilbert, B.; Huang, F.; Zhang, H. Z.; Waychunas, G. A.; Banfield, J. F., Nanoparticles: Strained and stiff. *Science* **2004,** 305, (5684), 651-654.

(17) Dubiel, M.; Brunsch, S.; Seifert, W.; Hofmeister, H.; Tan, G. L., Stress state of silver nanoparticles embedded in a silicate glass matrix investigated by HREM and EXAFS spectroscopy. *European Physical Journal D* **2001,** 16, (1-3), 229-232.

(18) Dubiel, M.; Schneider, R.; Hofmeister, H.; Schicke, K. D.; Pivin, J. C., Formation of argentic clusters and small Ag nanoparticles in soda-lime silicate glass. *European Physical Journal D* **2007,** 43, (1-3), 291-294.

(19) Pedersen, J. S., Analysis of small-angle scattering data from colloids and polymer solutions: modeling and least-squares fitting. *Advances in Colloid and Interface Science* **1997,** 70, 171-210.
(20) Glatter, O.; Kratky, O., *Small Angle X-ray Scattering*. ed.; Academic Press: 1982.
(21) Greaves, G. N.; Bras, W.; Oversluizen, M.; Clark, S. M., A SAXS/WAXS XAFS study of crystallisation in cordierite glass. *Faraday Discussions* **2003,** 122, 299-314.
(22) Durville, F.; Champagnon, B.; Duval, E.; Boulon, G.; Gaume, F.; Wright, A. F.; Fitch, A. N., Nucleation Induced In A Cordierite Glass By Cr-3+ - A Study By Small-Angle Neutron-Scattering, Electron-Paramagnetic Resonance And Laser Spectroscopy. *Physics And Chemistry Of Glasses* **1984,** 25, (5), 126-133.
(23) Mittelbach, R.; Glatter, O., Direct structure analysis of small-angle scattering data from polydisperse colloidal particles. *Journal of Applied Crystallography* **1998,** 31, 600-608.
(24) Megens, M.; vanKats, C. M.; Bosecke, P.; Vos, W. L., In situ characterization of colloidal spheres by synchrotron small-angle x-ray scattering. *Langmuir* **1997,** 13, (23), 6120-6129.
(25) Wignall, G. D., Neutron and X-ray scattering. In *Physical properties of polymers*, JE, M., Ed. AIP: Woodbury, 1996; pp 299-312.
(26) Bamford, H.; Tipper, C., In *Comprehensive chemical kinetics*, Bamford, H.; Tipper, C., Eds. Elsevier N.Y. : 1980; Vol. 22 chapter 3.
(27) Cumming, A.; Wiltzius, P.; Bates, F. S.; Rosedale, J. H., Light-Scattering Experiments on Phase-Separation Dynamics in Binary Fluid Mixtures. *Physical Review A* **1992,** 45, (2), 885-897.
(28) Rao, P.; Doremus, R., Kinetics of growth of nanosized gold clusters in glass. *Journal of Non-Crystalline Solids* **1996,** 203, 202-205.
(29) Wagner, R.; Kampmann, R., *Homogeneous second phase precipitation*. VCH: 1991; Vol. 5.
(30) Dong, J. P.; Chen, W.; Luo, L., Effects of Cr2O3 additive on crystallization behavior of MgO-Al2O3-SiO2-TiO2 glass-ceramics. *Journal of Inorganic Materials* **2006,** 21, (5), 1060-1066.
(31) Donald, I. W., The Crystallization Kinetics of a Glass Based on the Cordierite Composition Studied by Dta and Dsc. *Journal of Materials Science* **1995,** 30, (4), 904-915.
(32) Birch, F., Finite elastic strain of cubic crystals. *Phys. rev. A* **1947,** 71, 809-924.
(33) Suzuki, I.; Ohno, I.; Anderson, O. L., Harmonic and anharmonic properties of spinel MgAl2O4. *American Mineralogist* **2000,** 85, (2), 304-311.
(34) Martignago, F.; Negro, A. D.; Carbonin, S., How Cr3+ and Fe3+ affect MG-AL order-disorder transformation at high temperatures in spinel. *Phys Chem Minerals* **2003,** 30, 401-408.
(35) Tauch, D.; Russel, C., Glass-ceramics with zero thermal expansion in the system BaO/Al2O3/B2O3. *Journal of Non-Crystalline Solids* **2005,** 351, (27-29), 2294-2298.
(36) Perebeinos, V.; Chan, S. W.; Zhang, F., 'Madelung model' prediction for dependence of lattice parameter on nanocrystal size. *Solid State Communications* **2002,** 123, (6-7), 295-297.
(37) Belova, N. S.; Rempel, A. A., PbS nanoparticles: Synthesis and size determination by X-ray diffraction. *Inorganic Materials* **2004,** 40, (1), 3-10.
(38) Borrelli, N. F.; Hall, D. W.; Holland, H. J.; Smith, D. W., Quantum Confinement Effects Of Semiconducting Microcrystallites In Glass. *Journal Of Applied Physics* **1987,** 61, (12), 5399-5409.

For table of contents only

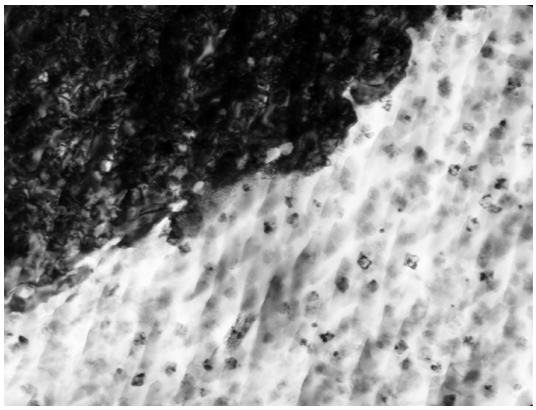

Utilising a multitude of experimental techniques it has been possible to elucidate the growth process of two crystalline phases in a glassy cordierite matrix